

Structural 130-K Phase Transition and Emergence of a Two-Ion Kondo State in HT-Ce₂Rh₂Ga Explored by ^{69,71}Ga Nuclear Quadrupole Resonance

Sh. Yamamoto,^{1,2,*} T. Fujii,² S. Luther,^{1,3} H. Yasuoka,² H. Sakai,⁴ F. Bärtl,^{1,3} K. M. Ranjith,² H. Rosner,² J. Wosnitza,^{1,3} A. M. Strydom,^{2,5} H. Kühne,¹ and M. Baenitz²

¹*Hochfeld-Magnetlabor Dresden (HLD-EMFL) and Würzburg-Dresden Cluster of Excellence ct.qmat, Helmholtz-Zentrum Dresden-Rossendorf, 01328 Dresden, Germany*

²*Max Planck Institute for Chemical Physics of Solid, D-01187 Dresden, Germany*

³*Institut für Festkörper- und Materialphysik, TU Dresden, 01062 Dresden, Germany*

⁴*Advanced Science Research Center, Japan Atomic Energy Agency, Tokai, Ibaraki 319-1195, Japan*

⁵*Highly Correlated Matter Research Group, Physics Department, University of Johannesburg, PO Box 524, Auckland Park 2006, South Africa*

(Dated: July 13, 2022)

We have studied the microscopic magnetic properties, the nature of the 130-K phase transition, and the ground state in the recently synthesized compound Ce₂Rh₂Ga by use of ^{69,71}Ga nuclear quadrupole resonance (NQR). The NQR spectra clearly show an unusual phase transition at $T_t \sim 130$ K yielding a splitting of the high-temperature single NQR line into two clearly resolved NQR lines, providing evidence for two crystallographically inequivalent Ga sites. The NQR frequencies are in good agreement with fully-relativistic calculations of the band structure. Our NQR results indicate the absence of magnetic or charge order down to 0.3 K. The temperature dependence of the spin-lattice relaxation rate, $1/T_1$, shows three distinct regimes, with onset temperatures at T_t and 2 K. The temperature-independent $1/T_1$, observed between T_t and 2 K, crosses over to a Korringa process, $1/T_1 \propto T$, below ~ 2 K, which evidences a rare two-ion Kondo scenario: the system goes into a dense Kondo coherent state at 2.0 and 0.8 K for the two different Ga sites.

Introduction. — Among the correlated $4f$ -ion systems, there are only a few compounds in which a structural instability at high temperatures has an effect on the ground state and especially on the correlations among the $4f$ ions and conduction electrons. While in Yb systems charge ordering or even significant intermediate-valence behavior can occur, Ce systems are usually characterized by a rather stable valence [1, 2]. Ce₂Rh₂Ga seems to be an exception to the rule. This material is dimorphic, with high- (HT) and low-temperature (LT) forms, yielding an orthorhombic La₂Ni₃-type (space group $Cmce$) and monoclinic (space group $C2/c$) structure at room temperature, respectively, depending on thermal treatments during the sample synthesis [3].

In the so-called HT-Ce₂Rh₂Ga form a structural phase transition at 130 K changes the ground state due to a reconstruction of the Fermi surface and a slight increase of the Ce valence beyond $3+$ [3–5]. The question arises how this influences the coupling of charge and spin. As a consequence of the 130-K phase transition, the coupling between the cerium ions is reduced [6], which is a prerequisite for the formation of the heavy-fermion state. Furthermore, the low-temperature phase exhibits two inequivalent Ce ions, which are exposed to Kondo screening at different temperatures. Multi-ion Kondo physics is rare and only poorly explored. Exceptions are theoretical studies [7–9] as well as experimental studies of site-dependent magnetic transitions for Ce₃Pd₂₀Si₆ [10], Ce₃PtIn₁₁ [11–13], and Ce₇Ni₃ [14]. Here, site-selective

microscopic experiments can provide crucial information for understanding the underlying physics.

In this Letter, we study the HT form, HT-Ce₂Rh₂Ga, which exhibits a unique phase transition at $T_t \sim 130$ K that is accompanied by signatures in the specific heat and susceptibility. Taking these anomalies into account, the authors in Ref. [3] argued that below T_t , HT-Ce₂Rh₂Ga undergoes an antiferromagnetic (AFM) order. Alternatively, a charge density wave (CDW) scenario is also possible. However, the origin of the 130-K phase transition is not yet fully understood.

The structural phase change across T_t has been studied by x-ray diffraction experiments [4]. The structure changes from a room-temperature orthorhombic phase ($a = 5.845$ Å, $b = 9.573$ Å, $c = 7.496$ Å) to a monoclinic phase with non-merohedral twinning of the space group $C2/m$ ($a = 9.401$ Å, $b = 5.807$ Å, $c = 7.595$ Å, $\beta = 91.89^\circ$). In the monoclinic phase below T_t , two inequivalent Ga sites are expected [4, 6]. Recent resonant x-ray emission spectroscopy experiments indicate that the average Ce valence, v , increases by ~ 0.7 % from the orthorhombic ($v \sim 3.053$) to the monoclinic ($v \sim 3.075$) phase [5]. In addition, our specific-heat data indicate the occurrence of a heavy-fermion state [6].

The aim of this Letter is to provide microscopic information on the nature of the 130-K phase transition, as well as on the formation of the correlated ground state. The present NQR results clearly show that neither an AFM nor CDW scenario can be considered. The symmetry reduction below 130 K yields two magnetically inequivalent Ce and Ga sites in the lattice. The NQR spin-lattice relaxation measured at these two Ga sites clearly indicates the formation of a heavy-fermion state, but the

* s.yamamoto@hzdr.de

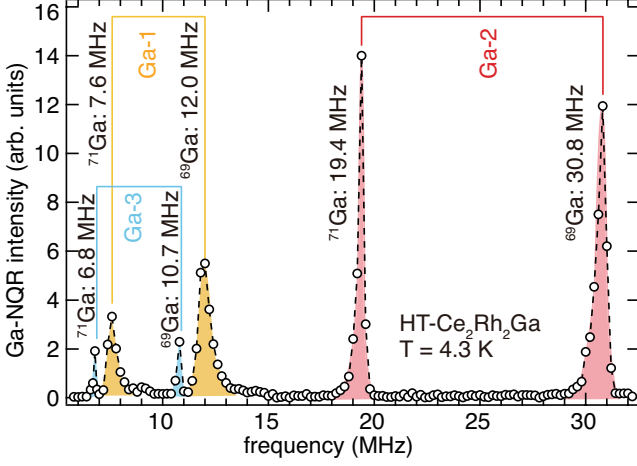


FIG. 1. Ga-NQR spectra of HT-Ce₂Rh₂Ga at 4.3 K. There are three pairs of ⁶⁹Ga and ⁷¹Ga NQR signals, Ga-1, 2, and 3, that are assigned to three inequivalent Ga sites.

transition to this occurs at two distinct temperatures. Thus, in CeRh₂Ga₂ there exist two cerium ions which are differently shielded by the surrounding conduction electrons (two-ion Kondo effect). The two cerium sublattices are magnetically coupled to each other. HT-Ce₂Rh₂Ga is, thus, a rather unusual 4f system which can serve as a platform to study the two-ion Kondo physics.

Experimental. — In this study, we focused on the Ga NQR in HT-Ce₂Rh₂Ga, where each Ce atom is surrounded by four Ga neighbors, forming edge-sharing CeGa₄ tetrahedra [6]. The sample was prepared in the same way as described in Ref. [3], i.e., the arc-melted ingot was annealed at 900 °C for 30 days in an evacuated quartz tube and then quenched in cold water. The annealed ingot was checked by x-ray diffraction to ensure the HT-Ce₂Rh₂Ga existence of the phase, and then powdered to about 200 μm particle size. The powdered sample was mixed with paraffin so that the skin-depth effect due to eddy currents by radio-frequency excitation during the NQR measurements is negligible [6].

The Ga nuclei have two stable isotopes, ⁶⁹Ga and ⁷¹Ga. Both of them have a nuclear spin of $I = 3/2$, and the nuclear gyromagnetic ratio, γ , the nuclear quadrupole moment, Q , and the natural abundance, A , are $^{69}\gamma = 10.2192 \text{ MHz/T}$, $^{69}Q = 0.178 \text{ barns}$, $^{69}A = 60 \%$ for ⁶⁹Ga, and $^{71}\gamma = 12.9847 \text{ MHz/T}$, $^{71}Q = 0.112 \text{ barns}$, $^{71}A = 40 \%$ for ⁷¹Ga, respectively. The ratios of γ and Q between the two isotopes are $(^{69}\gamma/^{71}\gamma) = 0.7870$ and $(^{69}Q/^{71}Q) = 1.589$. The NQR spectra and the nuclear relaxation times were measured using a standard pulsed (spin-echo) NMR apparatus (TecMag-Apollo). The NQR spectra were recorded by the frequency-sweep method. Further experimental details are described in Note 2 of the Supplemental Material [6].

Ga NQR spectra. — For searching the NQR signal, we consider the nuclear energy levels, E_m , obtained from the

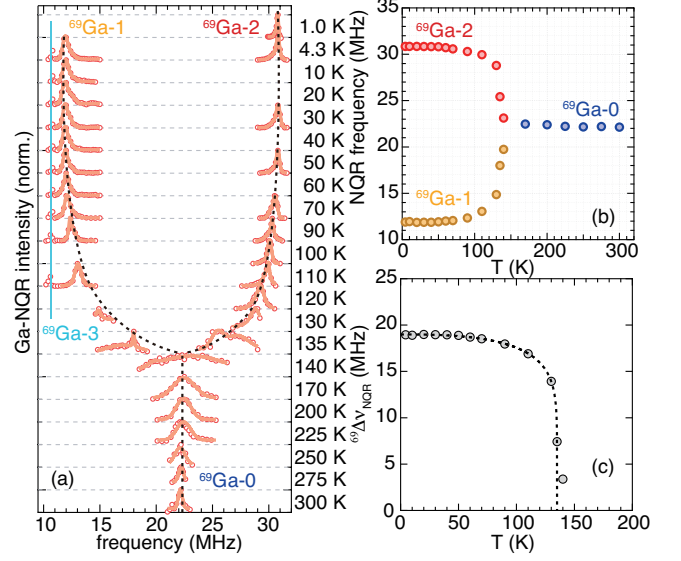


FIG. 2. (a) Temperature dependence of the ⁶⁹Ga-NQR spectra of HT-Ce₂Rh₂Ga. ⁶⁹Ga-0 is associated with the single Ga site in the orthorhombic phase ($T > T_t$), and the ⁶⁹Ga-1 and ⁶⁹Ga-2 signals stem from two inequivalent Ga sites in the monoclinic phase ($T < T_t$). (b) Temperature dependence of the ⁶⁹Ga-NQR peak frequencies extracted by using a Gaussian fit. Blue circles are data from ⁶⁹Ga-0 above T_t . Yellow and red circles are data from ⁶⁹Ga-1 and ⁶⁹Ga-2, respectively. (c) Temperature dependence of $^{69}\Delta\nu_{\text{NQR}} = f_Q(\text{Ga-2}) - f_Q(\text{Ga-1})$. The dashed line is a guide to the eye.

nuclear quadrupole Hamiltonian which can be expressed in the case of a nonaxial field gradient for $I = 3/2$ as [15],

$$E_{\pm 3/2} = \frac{1}{2} h \nu_Q \sqrt{1 + \frac{\eta^2}{3}}, \quad (1)$$

$$E_{\pm 1/2} = -\frac{1}{2} h \nu_Q \sqrt{1 + \frac{\eta^2}{3}}, \quad (2)$$

$$\nu_Q \equiv \frac{3e^2qQ}{h2I(2I-1)}, \quad (3)$$

where ν_Q denotes the quadrupole coupling between the electric-field gradient (EFG) stemming from an asymmetric charge distribution at the nuclear site, q , and the nuclear quadrupole moment, Q . The NQR occurs for the transition between two levels m and $m+1$, and the NQR frequency can be written as, $f_Q = \nu_Q(2m+1)/2$. Hence, only one NQR line for $I = 3/2$, ⁶⁹Ga and ⁷¹Ga, is expected.

In Fig. 1, we show a broad-band Ga NQR spectrum at 4.3 K (in the monoclinic phase). We observe three pairs of ⁶⁹Ga and ⁷¹Ga signals labeled Ga-1, Ga-2, and Ga-3. The observed frequency ratios for the NQR pairs ⁶⁹Ga and ⁷¹Ga NQR are 1.572 ± 0.005 , 1.589 ± 0.002 and 1.588 ± 0.010 , respectively. These numbers agree very well with the ratio of $^{69}Q/^{71}Q = 1.589$, confirming the validity of the spectral assignment.

TABLE I. Calculated EFG tensors and quadrupole coupling constants in HT-Ce₂Rh₂Ga (see main text). Ga-0 is associated with the Ga site in the orthorhombic phase above T_t . Ga-1 and Ga-2 are two inequivalent Ga sites in the monoclinic phase below T_t , respectively. The Wyckoff position for each Ga site is also shown.

Ga sites	Calculation				Experiment
	$V_{ZZ} = \partial V / \partial x_Z \partial x_Z$ (10^{21} V/m ²)	η	ν_Q (MHz)	ν_{NQR} (MHz)	ν_{NQR} (MHz)
Ga-0 (<i>Cmce</i> , 4a)	10.199	0.790	22.693	24.124	22.336
Ga-1 (<i>C2/m</i> , 2a)	-6.609	0.854	14.705	15.858	11.964
Ga-2 (<i>C2/m</i> , 2d)	13.197	0.652	29.363	30.346	30.758

Focusing on the ⁶⁹Ga NQR signal, we show the temperature dependence of the NQR spectrum in Fig. 2(a), including data above T_t (in the orthorhombic phase). The single Ga-NQR signal, ⁶⁹Ga-0, shows spectral broadening with decreasing temperature from 300 to 170 K, presumably due to some inhomogeneous distribution of the phase transition. Below ~ 130 K, the single peak Ga-0 splits into two lines, Ga-1 and Ga-2. We observe an additional Ga-NQR line, ⁶⁹Ga-3, at 10.8 MHz. Since the ⁶⁹Ga-3 signal yields a constant temperature dependence, we associate this with a signal either from twin boundaries or an impurity phase. The Ga-1 (Ga-2) peak shifts to lower (higher) frequency with decreasing temperature, reaching 12 MHz (30.8 MHz) at 4.3 K, see Fig. 2(b).

A question arises concerning the origin of the line splitting below T_t , because the first report of Ce₂Rh₂Ga proposed an AFM order below T_t [3]. However, if this would be the case, we would see an NQR line splitting due to the local hyperfine field from ordered Ce moments. As clearly seen in Fig. 2, we observe very sharp NQR lines for each Ga-1 and Ga-2 site at low temperatures, definitively affirming the absence of AF order. Further, as shown in the following, the temperature dependence of the spin-lattice relaxation rate does not display any peaks related to magnetic order [Fig. 3(a)], which excludes a possible scenario in which local fields from the Ce ions cancel each other at the Ga site. Preliminary μ SR measurements also support the absence of magnetic order above 2 K [18]. Furthermore, any spin and/or charge density wave order is excluded. In these cases, we should see a characteristic inhomogeneous line broadening due to the EFG or internal field modulation.

In order to check the site assignment above we performed EFG calculations based on the band structure calculated using the density functional theory solid-state code FPLO [16]. The k -meshes in both structures were carefully converged with respect to the total energy and the calculated EFG. We used the Perdew-Wang parametrization of the local density approximation for the exchange-correlation functional [17]. To account for the strong electronic correlations of the Ce 4*f* electrons, we applied the LDA+U approach with $U = 6$ eV for the Ce 4*f* states. Varying U by ± 1 eV did not show significant changes. Alternatively, treating the Ce 4*f* electron as a core state in the frozen core approximation yields very similar results for the EFG's on the Ga sites. The quadrupole coupling, ν_Q , can be obtained by calculating

the EFG at each Ga nuclear site which is defined as the second partial derivative of the electrostatic potential at the position of the nucleus. We summarized the obtained maximum EFG, V_{ZZ} , asymmetry parameter [$\eta = (V_{XX} - V_{YY})/V_{ZZ}$], and the quadrupole-coupling constant ν_Q in Table I. We compare then the extracted NQR frequencies with the experimental values. Thereby, we used $\nu_{\text{NQR}} = \nu_Q(1 + \eta^2/3)^{1/2}$ for $I = 3/2$. The NQR frequencies obtained from our experiments are in good agreement with the calculated values, assuring that the site assignment is correct.

Our specific-heat and susceptibility results signal a first-order transition in a narrow temperature region around T_t [3, 6]. On the other hand, a gradual variation of the NQR frequency has been observed from T_t down to ~ 80 K. Below T_t , the variation of the NQR frequencies couples predominantly to the evolving structural monoclinicity. The temperature-dependent splitting of the NQR spectra can be evaluated as $^{69}\Delta\nu_{\text{NQR}} = f_Q(\text{Ga-2}) - f_Q(\text{Ga-1})$, and is depicted in Fig. 2(c). The lattice parameters [3], and Ce 4*f* valence [5] also display a continuous variation with respect to temperature similar to that of the NQR frequency below T_t .

Nuclear magnetic relaxation. — The nuclear spin-lattice relaxation time, T_1 , has been measured by the inversion-recovery method, where the recovery of the nuclear magnetization, measured by the spin-echo amplitude after the application of an inversion pulse, $M(t)$, recovers as a single-exponential function for $I = 3/2$, and was fitted by the following function,

$$M(t) = M_0 [1 - c_0 \exp(-(3t/T_1)^\beta)], \quad (4)$$

where M_0 , c_0 , t , and β are the equilibrium nuclear magnetization, inversion factor ($c_0 = 2$ for complete inversion), the time after the inversion pulse, and the stretching exponent [6], respectively. We show the temperature dependences of $1/T_1$ for the ⁶⁹Ga-0, ⁶⁹Ga-1, and ⁶⁹Ga-2 lines in Fig. 3(a). There are three distinct temperature regions where the relaxation processes have different characteristic features: Regions I and II below T_t are in the monoclinic phase, while region III above T_t is in the orthorhombic phase. Before discussing the mechanism in each region, we have to clarify if the origin of the relaxation mechanism is magnetic or quadrupolar. The ratio of T_1 for the two isotopes, ⁷¹Ga and ⁶⁹Ga, is plotted in Fig. 3(b). As can be seen in the figure, the ratio is 0.6

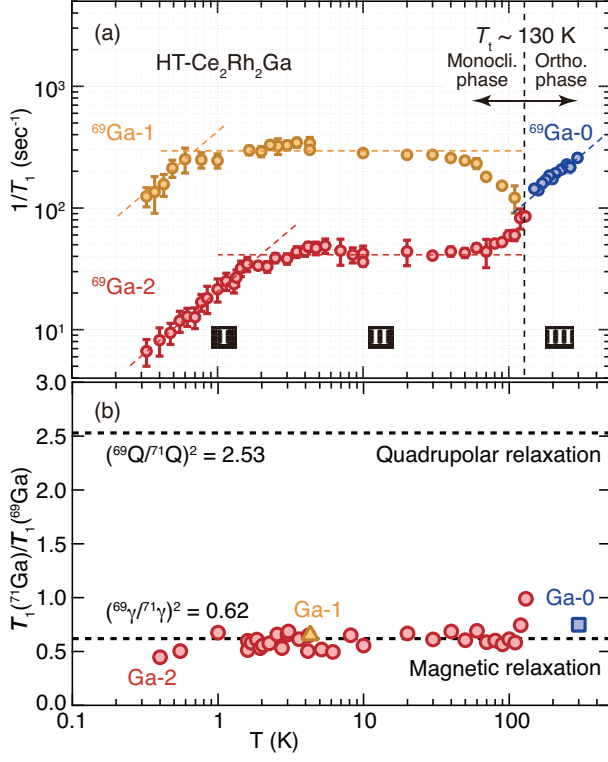


FIG. 3. (a) Temperature dependence of the ^{69}Ga -NQR spin-lattice relaxation rate, $1/T_1$, for the ^{69}Ga -0 (blue), ^{69}Ga -1 (yellow) and ^{69}Ga -2 (red) lines. There are three distinct temperature regions where the relaxation processes yield a different characteristic behavior. Region III is in the orthorhombic phase above $T_t \sim 130$ K and $1/T_1$ behaves like for a Korringa process. Region I and II lie within the monoclinic phase below T_t . (b) The ratio of T_1 for the two Ga isotopes, $^{71}\text{Ga}/^{69}\text{Ga}$, for the Ga-0, Ga-1, and Ga-2 lines are shown by blue, yellow, and red symbols, respectively.

for all temperatures, which is just equal to $(^{69}\gamma/^{71}\gamma)^2$, assuring that the relaxation process is governed by magnetic fluctuations, and not by fluctuations of the EFG (a quadrupolar relaxation process would give a ratio of 2.5). In the present case of a purely magnetic relaxation process, the relaxation rate, $1/T_1$, is generally expressed as [19],

$$\frac{1}{T_1} = \frac{k_B T}{(\gamma_e \hbar)^2} 2(\gamma_N A_\perp)^2 \sum_{\mathbf{q}} f^2(\mathbf{q}) \frac{\text{Im}\chi_\perp(\mathbf{q}, \omega_0)}{\omega_0}, \quad (5)$$

where γ_e , $\text{Im}\chi_\perp(\mathbf{q}, \omega_0)$, and ω_0 are the electronic gyromagnetic ratio, the perpendicular component of the imaginary part of the dynamical susceptibility, $\chi(\mathbf{q}, \omega_0)$, with respect to the quantization axis, and the nuclear Larmor frequency, respectively. $f(\mathbf{q})$ is the hyperfine form factor.

For $4f$ metals such as $\text{Ce}_2\text{Rh}_2\text{Ga}$, we have two relaxation channels: one from electron-hole pair excitations across the Fermi level and the other is due to exchange-

coupled Ce local spin fluctuations. For the former case, $\chi(\mathbf{q}, \omega_0)$ is temperature independent and $f(\mathbf{q}) = 1$, hence, $1/T_1 \propto T$ (Korringa process) [20], while in the latter case, $\chi(\mathbf{q}, \omega_0)$ may yield a strong \mathbf{q} and temperature dependence, depending on ferro- or antiferromagnetic correlations. In such a case, we have a temperature-independent relaxation process, $1/T_1 \propto A^2 J(J+1)/3\omega_{ex}$, where $J\mu_B$ is the Ce localized moment and ω_{ex} is the exchange frequency, which is estimated from the Weiss constant of the Curie-Weiss (CW) susceptibility [21, 22]. Since the bulk susceptibility of HT- $\text{Ce}_2\text{Rh}_2\text{Ga}$ shows a CW temperature dependence with a Weiss constant $\theta_p \sim -140$ K in the orthorhombic phase [3, 6], the primary relaxation process is considered to stem from AF spin fluctuations.

$F(\mathbf{q})$, the q -summed $f^2(\mathbf{q})$, should be calculated from the local geometrical factor at the Ga site [6]. We start to discuss region III, where we see the Korringa behavior $1/T_1 \propto T$. This is not compatible with the localized picture of exchange-coupled $4f$ Ce^{3+} moments. We calculate that the hyperfine form factor $F(\pi, \pi, \pi)$ is approximately $1/64$ of $F(0, 0, 0)$, by assuming an isotropic hyperfine coupling constant between the Ga and Ce ions in the orthorhombic phase, taking into account the Ce ions up to the third-nearest neighbor of the Ga ion [6]. Correspondingly, the contribution of AF fluctuations to $1/T_1$ is strongly suppressed due to the form factor in region III, and the Korringa process exceeds the contribution by AF fluctuations, which results in the found linear temperature dependence of $1/T_1$.

Because of the lowering of the local symmetry at the Ga sites below T_t (monoclinic phase), one can expect that the AF fluctuations are not screened in region II, which results in the temperature-independent relaxation process via fluctuations of the local Ce moment contributions at the Ga-1 and Ga-2 sites. In region I, $1/T_1$ exhibits again a Korringa behavior below 0.8 K for Ga-1 and below 2.0 K for Ga-2. This crossover of the relaxation process firmly indicates that the Ce $4f$ state is strongly hybridized with the conduction electrons, forming a coherent heavy-electron state, i.e., a dense Kondo coherent state. This formation of a Kondo coherent state has also been reported from measurements of temperature-dependent $1/T_1$ for other Ce-based heavy fermions [23]. It is worth to point out that the coherence temperature is different for Ga-1 (~ 0.8 K) and Ga-2 (~ 2.0 K). This presumably results from different Kondo screening, i.e., different Kondo temperatures for the two inequivalent Ce ions. Specific-heat results obtained on HT- $\text{Ce}_2\text{Rh}_2\text{Ga}$ polycrystals also indicate the formation of a heavy-fermion state with a Sommerfeld coefficient $\gamma = 1$ J/mol f.u. K² [6].

Conclusion. — We investigated the microscopic nature of the 130-K phase transition and the formation of the unusual ground state of HT- $\text{Ce}_2\text{Rh}_2\text{Ga}$ using NQR. The spectral variation with temperature across $T_t \sim 130$ K provides evidence for the absence of magnetic or charge order. The temperature dependence of $1/T_1$ is governed by the antiferromagnetically coupled Ce- $4f$ local spin

fluctuations, but both above T_c , and below 0.8 K for the Ga-1 site and below 2.0 K for the Ga-2 site, $1/T_1(T)$ behaves Korringa-like. Here, we argue that the former is due to the screening of the AF fluctuations by the hyperfine form factor, and the latter is due to the formation of a Kondo coherent state. Particularly, the emergence of a two-ion Kondo state with inequivalent Ce ions being screened at different temperatures is the most important outcome of the present study. It can be assumed that the Fermi surface is very anisotropic in $\text{Ce}_2\text{Rh}_2\text{Ga}$, which makes future studies of single crystals very interesting. A spatially anisotropic conductivity limits the RKKY interaction in real space, and, thus, affects the competition with the isotropic Kondo interaction. This creates an anisotropic Kondo system with multi-ion Kondo physics, which is certainly an exciting topic for future studies.

ACKNOWLEDGMENTS

We thank A. Tursina for fruitful discussions and for leading our understanding of the crystal structure of the title compound. U. Nitsche is acknowledged for technical support. We acknowledge the support of the HLD at HZDR, member of the European Magnetic Field Laboratory (EMFL), the Deutsche Forschungsgemeinschaft (DFG) through SFB 1143, and the Würzburg-Dresden Cluster of Excellence on Complexity and Topology in Quantum Matter–*ct.qmat* (EXC 2147, Project ID 390858490). A.M.S. thanks the NRF (93549) and the URC/FRC of UJ for financial assistance.

-
- [1] N. B. Brandt, and V. V. Moshchalkov, Concentrated Kondo systems, *Adv. Phys.* **33**, 373 (1984).
 - [2] A. C. Hewson, D. M. Newns, J. W. Rasul, N. Read, H. U. Desgranges, and P. Strange, Models for Intermediate Valence Systems and Kondo Lattices - Applications to Cerium and Ytterbium Compounds, In: T. Kasuya, and T. Sato. (eds) *Theory of Heavy Fermions and Valence Fluctuations*. Springer Series in Solid State Sciences, vol 62. Springer, Berlin, Heidelberg (1985).
 - [3] S. Nesterenko, A. Tursina, M. Pasturel, S. Xhakaza, and A. Strydom, Two polymorphs of a new intermetallic $\text{Ce}_2\text{Rh}_2\text{Ga}$ —crystal structure and physical properties, *J. Alloys Compd.* **844**, 155570 (2020).
 - [4] A. Dudka, S. Nesterenko, and A. Tursina, Multi-temperature X-ray diffraction study of a reversible structural phase transition in the high-temperature polymorph of $\text{Ce}_2\text{Rh}_2\text{Ga}$ compound, *J. Alloys Compd.* **890**, 161759 (2022).
 - [5] H. Sato, T. Matsumoto, N. Kawamura, K. Maeda, T. Takabatake, and A. M. Strydom, Valence transition of the intermetallic compound $\text{Ce}_2\text{Rh}_2\text{Ga}$ probed by resonant x-ray emission spectroscopy, *Phys. Rev. B* **105**, 035113 (2022).
 - [6] See Supplemental Material at <http://link.aps.org/supplemental/...> for the crystal structures of HT- $\text{Ce}_2\text{Rh}_2\text{Ga}$, experimental details of the NQR measurements, the calculation of $f(q)$, and macroscopic data, which includes Refs. [3–5].
 - [7] P. A. Lee, T. M. Rice, J. W. Serene, L. J. Sham, and J. W. Wilkins, Theories of heavy-electron systems, *Comments Condens. Matter Phys.* **12**, 99 (1986).
 - [8] A. Benlagra, L. Fritz, and M. Vojta, Kondo lattices with inequivalent local moments: Competitive versus cooperative Kondo screening, *Phys. Rev. B*, **84**, 075126 (2011).
 - [9] M. Jiang, Enhanced antiferromagnetic ordering tendency in the staggered periodic Anderson model, *Phys. Rev. B* **101**, 235124 (2020).
 - [10] S. Paschen, M. Müller, J. Custers, M. Kriegisch, A. Prokofiev, G. Hilscher, W. Steiner, A. Pikul, F. Steglich, and A. M. Strydom, Quantum critical behaviour in $\text{Ce}_3\text{Pd}_{20}\text{Si}_6$?, *J. Magn. Magn. Mater.* **316**, 90 (2007).
 - [11] J. Prokleška, M. Kratochvílová, K. Uhlířová, V. Sechovský, and J. Custers, Magnetism, superconductivity, and quantum criticality in the multisite cerium heavy-fermion compound $\text{Ce}_3\text{PtIn}_{11}$, *Phys. Rev. B* **92**, 161114, (2015).
 - [12] S. Kambe, H. Sakai, Y. Tokunaga, R. E. Walstedt, M. Kratochvílová, K. Uhlířová, and J. Custers, ^{115}In NQR study with evidence for two magnetic quantum critical points in dual Ce site superconductor $\text{Ce}_3\text{PtIn}_{11}$, *Phys. Rev. B* **101**, 081103 (2020).
 - [13] H. Fukazawa, K. Kumeda, N. Shioda, Y. Lee, Y. Kohori, K. Sugimoto, D. Das, J. Blawat, and D. Kaczorowski, Successive magnetic transitions in the heavy-fermion superconductor $\text{Ce}_3\text{PtIn}_{11}$ studied by ^{115}In nuclear quadrupole resonance, *Phys. Rev. B* **102**, 165124 (2020).
 - [14] K. Umeo, Y. Echizen, M. H. Jung, T. Takabatake, T. Sakakibara, T. Terashima, C. Terakura, C. Pfleiderer, M. Uhlarz, and H. v. Löhneysen, Field-induced magnetic transition in the heavy-fermion antiferromagnet Ce_7Ni_3 , *Phys. Rev. B* **67**, 144408 (2003).
 - [15] T. P. Das and E. L. Hahn, *Nuclear Quadrupole Resonance Spectroscopy* (Academic Press Inc., New York, 1958)
 - [16] K. Koepnick, and H. Eschrig, Full-potential nonorthogonal local-orbital minimum-basis band-structure scheme, *Phys. Rev. B* **59**, 1743 (1999).
 - [17] J. P. Perdew, and Y. Wang, Accurate and simple analytic representation of the electron-gas correlation energy, *Phys. Rev. B* **45**, 13244 (1992).
 - [18] A. M. Strydom, private communication, ISIS μSR experimental report 2010475.
 - [19] T. Moriya, The effect of electron-electron interaction on the nuclear spin relaxation in metals, *J. Phys. Soc. Jap.* **18**, 516 (1963).
 - [20] J. Korringa, Nuclear magnetic relaxation and resonance line shift in metals, *Physica* **16**, 601 (1950).
 - [21] T. Moriya, Nuclear magnetic relaxation in antiferromagnetics, *Prog. Theor. Phys.* **16**, 23 (1956).
 - [22] T. Moriya, Nuclear magnetic relaxation in antiferromagnetics, II, *Prog. Theor. Phys.* **16**, 641 (1956).
 - [23] Y. Kawasaki, K. Ishida, Y. Kitaoka, and K. Asayama, K, Si-NMR study of antiferromagnetic heavy-fermion com-

pounds CePd_2Si_2 and CeRh_2Si_2 , Phys. Rev. B **58**, 8634 (1998).

Supplemental Material

Structural 130-K Phase Transition and Emergence of a Two-Ion Kondo State in HT-Ce₂Rh₂Ga Explored by ^{69,71}Ga Nuclear Quadrupole Resonance

Sh. Yamamoto,^{1,2,*} T. Fujii,² S. Luther,^{1,3} H. Yasuoka,² H. Sakai,⁴ F. Bärtl,^{1,3} K. M. Ranjith,² H. Rosner,² J. Wosnitza,^{1,3} A. M. Strydom,^{2,5} H. Kühne,¹ and M. Baenitz²

¹*Hochfeld-Magnetlabor Dresden (HLD-EMFL) and Würzburg-Dresden Cluster of Excellence ct.qmat, Helmholtz-Zentrum Dresden-Rossendorf, 01328 Dresden, Germany*

²*Max Planck Institute for Chemical Physics of Solid, D-01187 Dresden, Germany*

³*Institut für Festkörper- und Materialphysik, TU Dresden, 01062 Dresden, Germany*

⁴*Advanced Science Research Center, Japan Atomic Energy Agency, Tokai, Ibaraki 319-1195, Japan*

⁵*Highly Correlated Matter Research Group, Physics Department, University of Johannesburg, PO Box 524, Auckland Park 2006, South Africa*

(Dated: July 13, 2022)

We present here:

1. Crystal structure of HT-Ce₂Rh₂Ga
2. Experimental details of the NQR measurements
3. Calculation of the form factor in the orthorhombic phase of HT-Ce₂Rh₂Ga
4. Macroscopic data [susceptibility (χ vs T), magnetization (M vs H), and specific heat (C vs T and C_m/T vs T)] of polycrystalline HT-Ce₂Rh₂Ga

* s.yamamoto@hzdr.de

SUPPLEMENTARY NOTE 1:
Crystal structure of HT-Ce₂Rh₂Ga

HT-Ce₂Rh₂Ga crystallizes in the orthorhombic structure of La₂Ni₃ type (space group *Cmce*) above $T_t \sim 130$ K [S1]. Below T_t , the crystal structure changes to monoclinic (space group *C2/m*) being accompanied by non-merohedral twinning [S2]. Above T_t , there are single crystallographic sites for the Ce and Ga ions, while below T_t , there are two inequivalent Ce and Ga sites (Fig. S1). Bond lengths around Ga-0 in the orthorhombic *Cmce*, and Ga-1 (2a) and Ga-2 (2d) in the monoclinic *C2/m* phases are shown in Figs. S1(c), S1(d), and S1(e). Passing through the crystallographic phase transition from the high-temperature orthorhombic to low-temperature monoclinic phase at ~ 130 K, the average Ga-Ce bond length is reduced by 1.60 % and 0.12 % for the Ga-1 and Ga-2 sites, respectively.

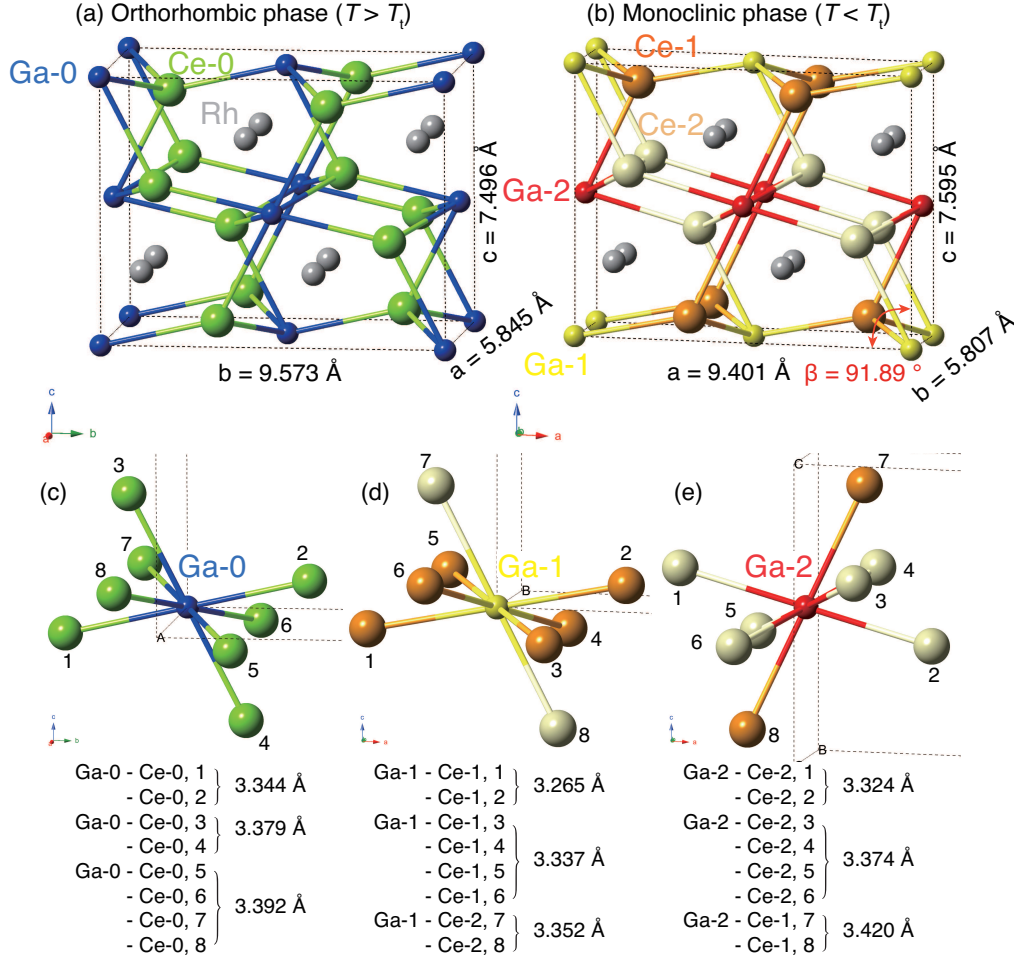


FIG. S1. Crystal structure of HT-Ce₂Rh₂Ga. (a) Orthorhombic phase above $T_t \sim 128$ K with La₂Ni₃-type (space group *Cmce*). (b) Monoclinic phase (space group *C2/m*) below T_t . Local coordination environment of 1st, 2nd, and 3rd nearest neighboring Ce atoms when viewed from (c) a Ga-0 (4a) atom in the orthorhombic *Cmce*, and (d) from a Ga-1 (2a) and (e) Ga-2 (2d) atom in the monoclinic *C2/m* phases. The bond lengths are also listed in (c), (d), and (e).

SUPPLEMENTARY NOTE 2: Experimental details of the NQR measurements

The $^{69,71}\text{Ga}$ NQR experiments were carried out with a high-quality powder sample prepared from the arc-melted single crystal. Using a 200 μm sieve, the particle size were selected to be less than 200 μm , and the obtained powder was mixed with paraffin. The NQR spectra and the nuclear magnetic relaxation times were measured using a standard pulsed (spin-echo) NMR apparatus (TecMag-Apollo).

The NQR spectra were taken by the frequency-sweep method under zero applied magnetic field. In order to avoid any artificial broadening, the real part of the spin-echo signal was integrated after proper phase adjustments at each frequency. The typical excitation-pulse width, two-pulse separation and repetition (t_r) time were 6 μsec , 30 μsec , and 100 msec, respectively. After several nutation experiments, the 6 μsec - 12 μsec pulse sequence was found to be the best for forming the spin-echo. From the typical 6 μsec exciting pulse width using a Cu coil (13-mm length and 2-mm radius), we can estimate that the radio-frequency (rf) field acting on the sample is of the order of 40 Oe. We used the temperature steps of 5 K and 10 K around T_t in our NQR spectral measurements.

As to a possible heating of the sample during the experiments, we calculated the skin-depth for a 30 MHz rf-field from the resistivity of $\text{Ce}_2\text{Rh}_2\text{Ga}$ in the monoclinic phase ($\sim 300 \mu\Omega \text{ cm}$) to be about 160 μm which is just about the maximum particle size of the sample. Therefore, the skin-depth effect due to eddy currents induced by rf excitation during the NQR measurements is considered to be negligible. We took special care not to heat the sample during the measurements, particularly in the ^3He temperature range. At selected temperatures, we measured the t_r dependence of the spin-echo (SE) intensity. Above a certain value t_r^T , the SE intensity becomes independent of t_r , where the increase of the sample temperature due to radio-frequency excitation is negligible. We used t_r which is at least twice as large as t_r^T .

The temperature dependence of the nuclear magnetic relaxation rate, $1/T_1$, was measured by the inversion-recovery method, where the evolution of the spin-echo amplitude after an inversion pulse was recorded as a function of the time interval between the inversion pulse and the first spin-echo pulse. The typical examples of the recovery curves are shown in Fig. S2(a) at 30 K (monoclinic phase), 130 K (close to the phase transition), and 297 K (orthorhombic phase). For $I = 3/2$, the recovery curve is described by Eq. (4) in the main text. Fig. S2(a) shows that all recovery curves are well described with a stretching exponent of $\beta = 1.0$, meaning the T_1 values are determined by a single relaxation process and no inhomogeneity is present at all temperatures. The error bars in Fig. 3(a) in the main text were extracted from the standard deviation of the fits to the recovery curves using Eq. (4). Figure S2(b) shows the temperature dependence of $1/T_1 T$. Three distinct temperature regions are seen.

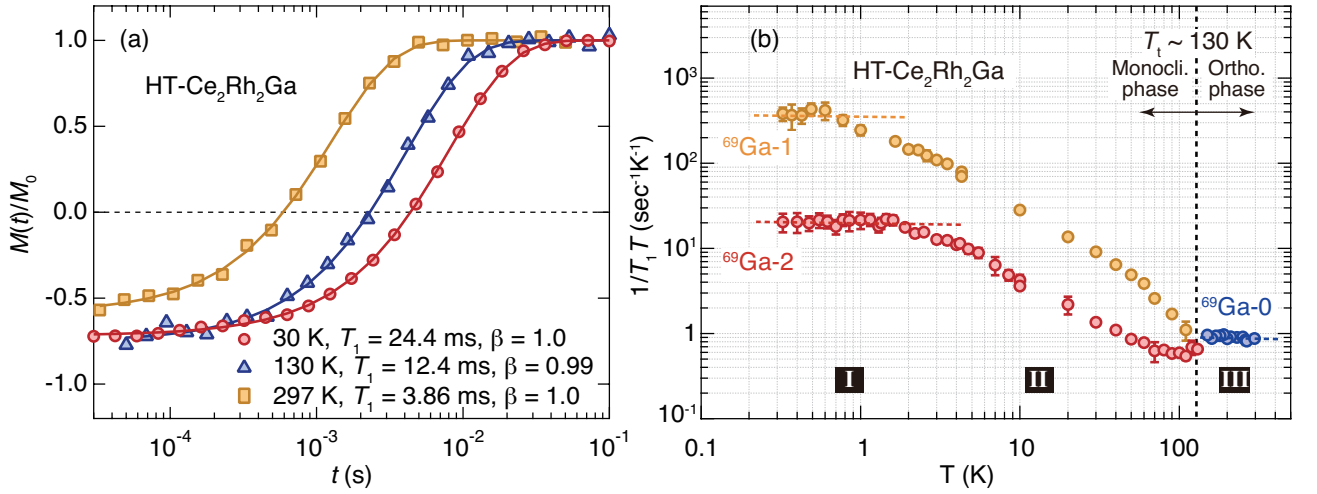


FIG. S2. (a) Recovery of ^{69}Ga nuclear magnetization $M(t)$ divided by the saturation value M_0 as a function of the delay t between the inversion and the first spin-echo pulses. The yellow, blue, and red symbols are data at 30 K, 130 K, and 297 K, which are below, close to, and above T_t , respectively. The solid lines are fits of recovery curves using Eq. (4). The stretching exponent β is ~ 1 at each temperature. (b) Temperature dependence of $1/T_1 T$, for the $^{69}\text{Ga-0}$ (blue), $^{69}\text{Ga-1}$ (yellow) and $^{69}\text{Ga-2}$ (red) lines.

SUPPLEMENTARY NOTE 3:

Calculation of the form factor of hyperfine coupling at the Ga sites of HT-Ce₂Rh₂Ga above T_t

In Eq. (5) of the main text, the \mathbf{q} -dependent hyperfine term $A_{\perp}^2 \Sigma_{\mathbf{q}} f^2(\mathbf{q})$ can often be approximated to $B_0^2 F(\mathbf{q})$, where B_0 is the averaged hyperfine coupling constant from the neighboring magnetic atoms and $F(\mathbf{q})$ is the \mathbf{q} -summed $f^2(\mathbf{q})$. $F(\mathbf{q})$ can be estimated from the local geometry as follows. For many intermetallic compounds, the hyperfine field is transferred by a RKKY-type mechanism with the local spins via conduction electrons. In such a case, the transferred hyperfine coupling constant would be inversely proportional to the cube of the distance ($\propto 1/r_i^3$) from the local spin. In HT-Ce₂Rh₂Ga, the Ga sites are located at the center of eight Ce atoms, as illustrated in Fig. S1(c). Assuming the same magnitude of B_0 from the surrounding Ce atoms, $F(\mathbf{q})$ can be numerically calculated from $\{\Sigma_i \exp(i\mathbf{q} \cdot \mathbf{r}_i)\}^2$, where \mathbf{r}_i is the local coordinate of each Ce atom with regard to the Ga sites. The calculated result is visualized in Fig. S3. $F(\mathbf{q})$ becomes much smaller at the AFM positions of $q_x = \pi$, $q_y = \pi$, and $q_z = \pi$ compared to $F(\mathbf{q} = 0)$, which results in the suppression of the contribution of AF fluctuations to $1/T_1$ in region III.

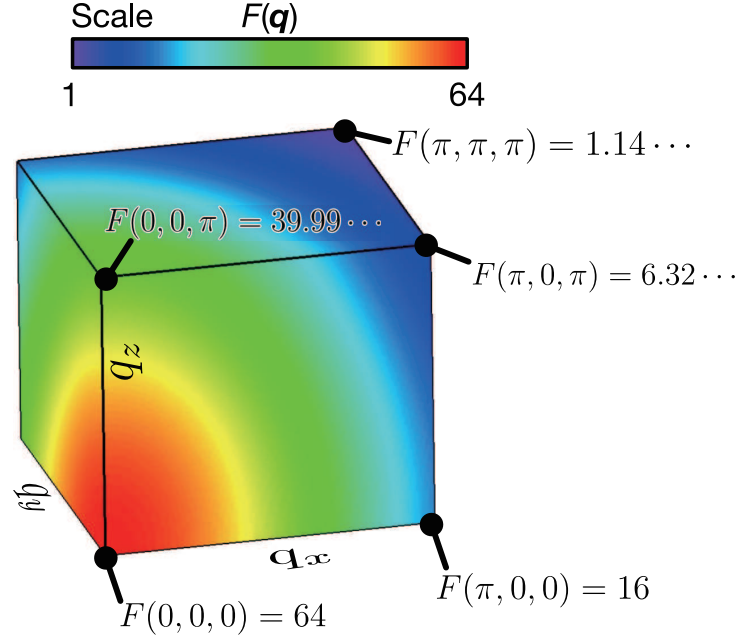


FIG. S3. Color scale plot of the Ga form factor in the unit of A_0^2 , where A_0 is the transferred hyperfine coupling constant. The A_0 is assumed to be uniform from the eight Ce-0 atoms [see Fig. S1(c)].

SUPPLEMENTARY NOTE 4:

Macroscopic data of polycrystalline HT-Ce₂Rh₂Ga

Among various macroscopic measurements on the sample used in the present NQR study, we show the temperature dependence of the static magnetic susceptibility [Fig. S4(a)], a lack of magnetic hysteresis at 2 K [Fig. S4(b)], and specific-heat measurements [Figs. S4(c) and S4(d)]. The magnitude of the Weiss constant θ_p obtained from the Curie-Weiss fit drastically changes across the structural phase transition. In addition, the Ce valence increases by ~ 0.7 % below T_t [S3]. These two experimental results evidence the reduction of the antiferromagnetic exchange interaction between the Ce ions below T_t . It should be emphasized here that the nearly temperature-independent magnetic specific heat, C_m/T , below 1.4 K provides strong evidence of the presence of a heavy-Fermi liquid state with $\gamma = 1$ J/mol_{f.u.}K² [Fig. S4(d)].

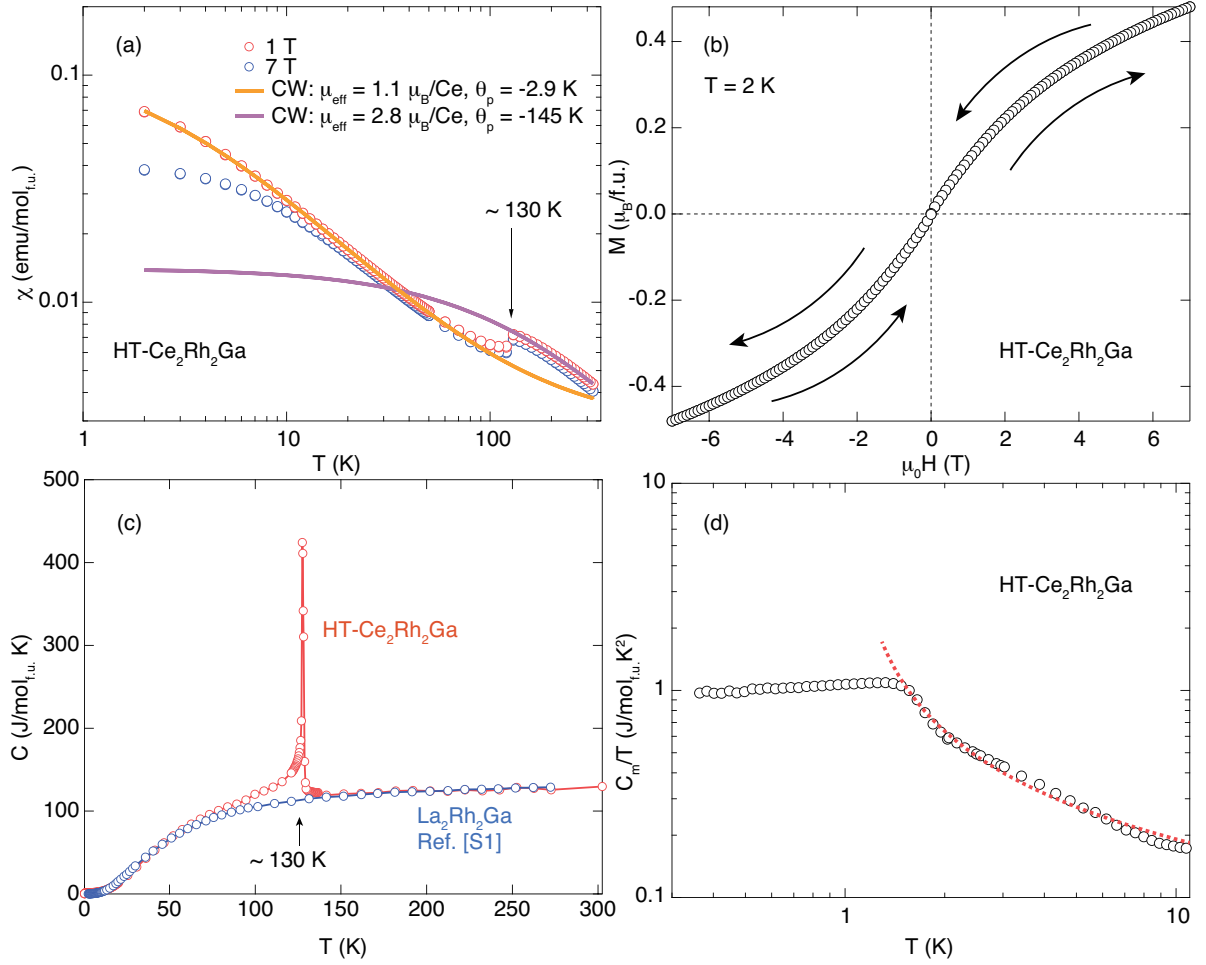


FIG. S4. (a) Susceptibility of polycrystalline HT-Ce₂Rh₂Ga as a function of temperature in magnetic fields of 1 and 7 T. The orange (purple) solid line represents a Curie-Weiss fit to the measured data below 50 K (above 150 K). The structural phase transition at ~ 130 K is clearly visible. (b) Magnetization of polycrystalline HT-Ce₂Rh₂Ga as a function of cycled magnetic fields between -7 T and +7 T at 2 K. No hysteresis associated with long-range order is visible. (c) Temperature dependence of the specific heat, C , for HT-Ce₂Rh₂Ga and its nonmagnetic relative La₂Rh₂Ga [S1]. The low-temperature magnetic specific heat, C_m , of Ce₂Rh₂Ga is determined by subtracting the contribution of La₂Rh₂Ga. (d) Extracted magnetic contribution C_m/T plotted against T in a log-log scale. The dashed curve is an empirical fit of the data to $c/\log(T)$ with $c = 0.19$. C_m/T is temperature independent below 1.4 K with the electronic specific heat, $\gamma = 1$ J/mol_{f.u.}K².

-
- [S1] S. Nesterenko, A. Tursina, M. Pasturel, S. Xhakaza, and A. Strydom, Two polymorphs of a new intermetallic $\text{Ce}_2\text{Rh}_2\text{Ga}$ —crystal structure and physical properties, *J. Alloys Compd.* **844**, 155570 (2020).
 - [S2] A. Dudka, S. Nesterenko, and A. Tursina, Multi-temperature X-ray diffraction study of a reversible structural phase transition in the high-temperature polymorph of $\text{Ce}_2\text{Rh}_2\text{Ga}$ compound, *J. Alloys Compd.* **890**, 161759 (2022).
 - [S3] H. Sato, T. Matsumoto, N. Kawamura, K. Maeda, T. Takabatake, and A. M. Strydom, Valence transition of the inter-metallic compound $\text{Ce}_2\text{Rh}_2\text{Ga}$ probed by resonant x-ray emission spectroscopy, *Phys. Rev. B* **105**, 035113 (2022).